Pergamon

0045-7949(95)00011-9

Computers & Structures Vol. 56, No. 5, pp. 825–835, 1995

0045-7949/95 $9.50 + 0.00

AN INVERSE METHOD FOR FINDING UNKNOWN SURFACE TRACTIONS AND DEFORMATIONS IN ELASTOSTATICS

T. J. Martin, J. D. Halderman and **G. S. Dulikravich**

Department of Aerospace Engineering, 233 Hammond Building, The Pennsylvania State University, University Park, PA 16802, U.S.A.

Abstract—We have developed a non-iterative algorithm for determining unknown deformations and tractions on surfaces of arbitrarily shaped solids where these quantities cannot be measured or evaluated. For this inverse boundary value technique to work, both deformations and tractions must be available and applied simultaneously on at least a part of the object's surface called an over-specified boundary. Our method is non-iterative only because it utilizes the boundary element method (BEM) to calculate deformations and tractions on surfaces where they are unavailable and simultaneously computes the stress and deformation field within the entire object. Inversely computed displacement and stress fields within simple solids and on their boundaries were in excellent agreement with the BEM analysis results and analytic solutions. Our algorithm is highly flexible in treating complex geometries and mixed elastostatics boundary conditions. The accuracy and reliability of this technique deteriorates when the known surface conditions are only slightly over-specified and far from the inaccessible surfaces.

INTRODUCTION

The objective of our steady-state inverse elastostatics problem is to deduce displacements and tractions on any surfaces or surface elements where such information is unknown. It is often difficult and even impossible to place strain gauges and take measurements on a particular surface of a solid body either due to its small size or geometric inaccessibility or because of the severity of the environment on that surface. With our inverse method these unknown elastostatics boundary values are deduced from additional displacement and surface traction measurements made at a finite number of points within the solid or on some other surfaces of the solid. Our approach is robust and fast since it is non-iterative. A similar inverse boundary value formulation has been shown [1–5] to compute meaningful and accurate thermal fields during a single analysis using a straightforward modification to the boundary element method (BEM) non-linear heat conduction analysis code and electric potential field.

It should be pointed out that the types of inverse problems to be discussed in this paper are conceptually different from a more familar inverse shape design problem [6–8] and from the unsteady inverse heat conduction problem [9–11]. These methods are iterative and inherently unstable thus requiring complex regularization algorithms [12]. Our inverse boundary value method is non-iterative only because it uses the BEM. If finite difference, finite element, spectral element or some other non-integral formulation is used instead of the BEM, our inverse boundary condition method would become iterative.

The BEM is a very accurate and efficient technique [13, 14] that can solve boundary value problems such as those governing heat conduction, electromagnetic fields, fluid flow, elasticity and many other physical phenomena. When analyzing steady-state elasticity problems using the BEM, either displacement vectors, **u**, or surface traction vectors, **p**, are specified everywhere on the surface of the solid where one of these quantities is known while the other is unknown. When performing an inverse evaluation of the steady-state elasticity problem using the BEM, both **u** and **p** must be specified on a part of the solid's surface, while both **u** and **p** are unknown on another part of the surface. Elsewhere on the solid's surface, either **u** or **p** should be applied. The surface section where both **u** and **p** are specified simultaneously is called the overspecified boundary.

ANALYTICAL AND NUMERICAL FORMULATION

The two-dimensional state of stress at a point is defined using a second order symmetric stress tensor, σ. These stress components must satisfy the following equilibrium equations [14] throughout the interior of the solid body shown here in indicial notation,

$$\frac{\partial \sigma_{kj}}{\partial x_j} + b_k = 0 \quad \text{where } j = 1, 2 \text{ and } k = 1, 2 \quad (1)$$

where b_k are the net body forces per unit volume. The surface force tractions on the object are denoted by the vector, p_k, and the prescribed boundary values of these tractions on the surface Γ_p are denoted by P_k. Equilibrium at the boundary requires

the satisfaction of the following stress boundary conditions [14]

$$p_k = \sigma_{kj} n_j = P_k \tag{2}$$

where n_j is the unit outward normal vector to the surface. The state of strain at a point within the solid is denoted by the second order symmetric strain tensor, ϵ. The strain–displacement relations for linear theory can be written in indicial form as

$$\epsilon_{kj} = \frac{1}{2}\left(\frac{\partial u_k}{\partial x_j} + \frac{\partial u_j}{\partial x_k}\right) \tag{3}$$

where u_k is the vector displacement field. Let Γ_u be the portion of the boundary where the displacement boundary conditions, U_k, are prescribed.

The states of stress and strain for a solid body are related through the stress–strain relations, also called Hooke's Law, which depend on the material behavior

$$\begin{Bmatrix} \epsilon_{xx} \\ \epsilon_{yy} \\ 2\epsilon_{yx} \end{Bmatrix} = \frac{1}{E}\begin{bmatrix} 1 & -\nu & 0 \\ -\nu & 1 & 0 \\ 0 & 0 & 2(1+\nu) \end{bmatrix}\begin{Bmatrix} \sigma_{xx} \\ \sigma_{yy} \\ \sigma_{yx} \end{Bmatrix} \tag{4}$$

where E is the Young's modulus of elasticity, ν is the Poisson's ratio and G is the shear modulus. Lame's constants are related to E and ν in the following way,

$$\lambda = \frac{E\nu}{(1+\nu)(1-2\nu)} \tag{5a}$$

$$G = \frac{E}{2(1+\nu)}. \tag{5b}$$

The principle of virtual displacements for linear elastic problems can be written as [14],

$$\int_\Omega \left(\frac{\partial \sigma_{kj}}{\partial x_j} + b_k\right) u_k^* \, d\Omega = \int_{\Gamma_p} (p_k - P_k) u_k^* \, d\Gamma + \int_{\Gamma_u} (U_k - u_k) \, p_k^* \, d\Gamma \tag{6}$$

where $p_k^* = n_j \sigma_{jk}^*$ are the surface tractions corresponding to the virtual displacements u_k^*. We will assume that the virtual strain–displacement relationships and the material properties are linear. After integrating by

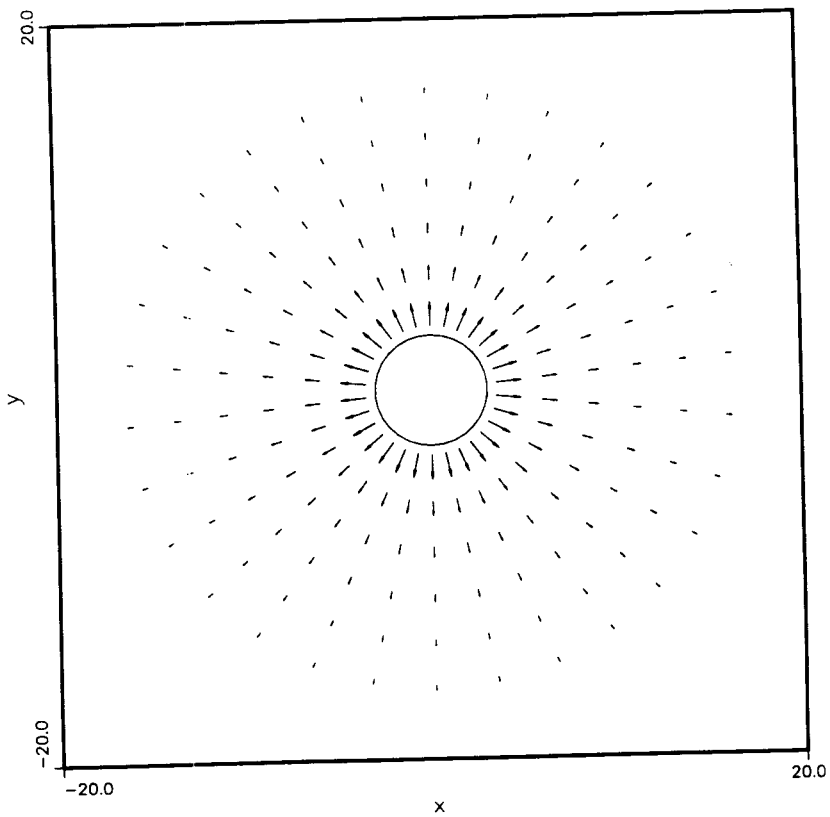

Fig. 1. Vector displacement field from the well-posed analysis of a pressurized circular cavity within an infinite plate.

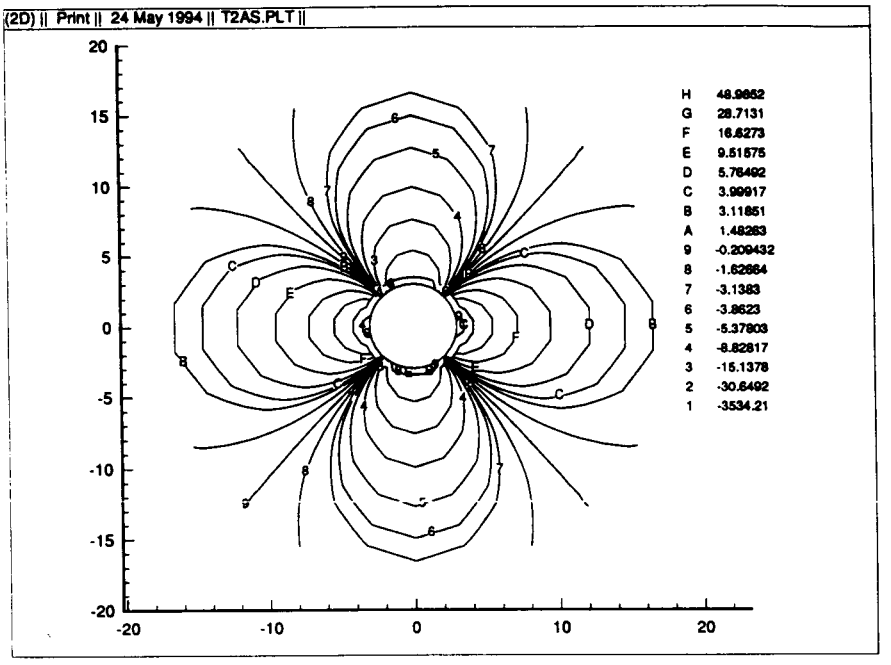

Fig. 2a. Contours of constant stresses, σ_{xx}, from the well-posed analysis of the pressurized circular cavity within an infinite plate.

parts twice and ignoring for now the body forces, we obtain

$$\int_\Omega \frac{\partial \sigma^*_{kj}}{\partial x_j} u_k \, d\Omega + \int_{\Gamma_p} P_k u^*_k \, d\Gamma + \int_{\Gamma_u} p_k u^*_k \, d\Gamma = \int_{\Gamma_u} U_k p^*_k \, d\Gamma + \int_{\Gamma_p} u_k p^*_k \, d\Gamma. \quad (7)$$

The virtual displacement will be a fundamental solution satisfying the equilibrium equations

$$\frac{\partial \sigma^*_{ij}}{\partial \zeta_j} + \delta_l(x_i - \zeta_i) = 0 \quad (8)$$

where δ is the Dirac's delta function and represents a unit load at the point "i" in the "l" direction. In

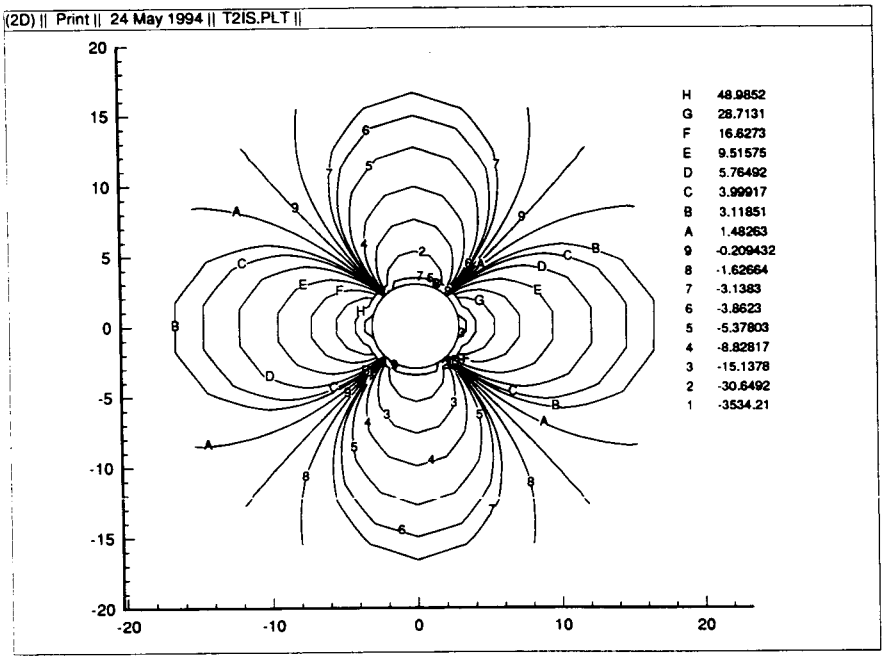

Fig. 2b. Contours of constant stresses, σ_{xx}, from the ill-posed analysis of the pressurized circular cavity within an infinite plate.

general, we can write for any point "i" and for each direction "l" a boundary integral equation

$$c^i u^i_l = \int_\Gamma u_k p u^*_{lk}\, d\Gamma = \int_\Gamma p_k u^*_{lk}\, d\Gamma \qquad (9)$$

where the term c_l is obtained with some special treatment of the surface integral on the left hand side [14]. Explicit calculation of this value can be obtained by augmenting the surface integral over the singularity that occurs when the integral includes the point "i". Fortunately, explicit calculation is not necessary as it can be obtained using the rigid body motions. The fundamental solution for two-dimensional isotropic plane strain case is

$$u^*_{lk} = \frac{1}{8\pi G(1-\nu)}\left[(3-4\nu)\ln\left(\frac{1}{r}\right)\Delta_{lk} + \frac{\partial r}{\partial x_l}\frac{\partial r}{\partial x_k}\right] \qquad (10)$$

where r is the distance from the "i" node to the point of integration on the boundary and Δ is the Kronecker delta.

The boundary Γ is discretized into N_{sp} flat surface panels connected between N nodes. The functions **u** and **p** are quadratically distributed over each panel with adjacent panels sharing nodes such that there will be twice as many boundary nodes as there are surface panels. A transformation from the global (x, y) coordinate system to a localized boundary fitted (ζ) coordinate system is required in order to numerically integrate each surface integral using Gaussian quadrature. The displacements and tractions are defined in terms of three nodal values and three quadratic interpolation functions. The whole set of boundary integral equations can be written in matrix form as

$$[\mathbf{H}]\{\mathbf{U}\} = [\mathbf{G}]\{\mathbf{P}\} \qquad (11)$$

where the vectors $\{\mathbf{U}\}$ and $\{\mathbf{P}\}$ contain the nodal values of the displacement and traction vectors. Each entry in the [**H**] and [**G**] matrices is developed by properly summing the contributions from each numerically integrated surface integral. The surface tractions were allowed to be discontinuous between each neighboring surface panel to allow for proper corner treatment. The set of boundary integral equations will contain a total of $2N$ equations and $6N$ nodal values of displacements and surface traction.

For a well-posed boundary value problem, at least one of the functions, **u** or **p**, will be known at each

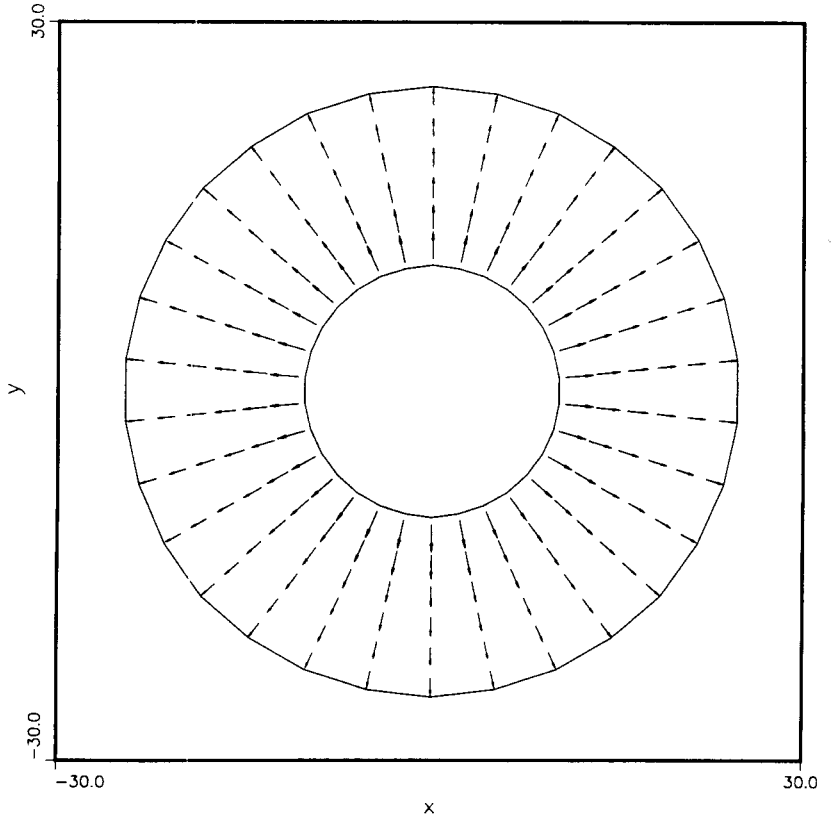

Fig. 3a. Vector displacement field from the well-posed analysis of an annular pressurized disk.

boundary node (either Dirichlet or von Neumann boundary condition) so that the equation set will be composed of $2N$ unknowns and $2N$ equations. Since there are two distinct traction vectors at corner nodes, the boundary conditions applied there should include either two tractions or one displacement and one traction. If only displacements are specified across a corner node, special treatment is required [13].

For an ill-posed boundary value problem, both $\mathbf{u}$ and $\mathbf{p}$ should be enforced simultaneously at certain boundary nodes, while either $\mathbf{u}$ or $\mathbf{p}$ should be enforced at the other boundary nodes, and nothing enforced at the remaining boundary nodes. For the simple example of a quadrilateral plate with four nodes, if at two boundary nodes both $\mathbf{u} = \mathbf{U}$ and $\mathbf{p} = \mathbf{P}$ are known, but at the other two nodes neither $\mathbf{u}$ or $\mathbf{p}$ is known, the BEM equation set before any rearrangement appears as

$$\begin{bmatrix} \mathbf{h}_{11} & \mathbf{h}_{12} & \mathbf{h}_{13} & \mathbf{h}_{14} \\ \mathbf{h}_{21} & \mathbf{h}_{22} & \mathbf{h}_{23} & \mathbf{h}_{24} \\ \mathbf{h}_{31} & \mathbf{h}_{32} & \mathbf{h}_{33} & \mathbf{h}_{34} \\ \mathbf{h}_{41} & \mathbf{h}_{42} & \mathbf{h}_{43} & \mathbf{h}_{44} \end{bmatrix} \begin{Bmatrix} \mathbf{U}_1 \\ \mathbf{u}_2 \\ \mathbf{U}_3 \\ \mathbf{u}_4 \end{Bmatrix}$$

$$= \begin{bmatrix} \mathbf{g}_{11} & \mathbf{g}_{12} & \mathbf{g}_{13} & \mathbf{g}_{14} \\ \mathbf{g}_{21} & \mathbf{g}_{22} & \mathbf{g}_{23} & \mathbf{g}_{24} \\ \mathbf{g}_{31} & \mathbf{g}_{32} & \mathbf{g}_{33} & \mathbf{g}_{34} \\ \mathbf{g}_{41} & \mathbf{g}_{42} & \mathbf{g}_{43} & \mathbf{g}_{44} \end{bmatrix} \begin{Bmatrix} \mathbf{P}_1 \\ \mathbf{p}_2 \\ \mathbf{P}_3 \\ \mathbf{p}_4 \end{Bmatrix} \tag{12}$$

where each of the entries in the [H] and [G] matrices is a 2×2 submatrix.

Straightforward algebraic manipulation yields the following set

$$\begin{bmatrix} \mathbf{h}_{12} & -\mathbf{g}_{12} & \mathbf{h}_{14} & -\mathbf{g}_{14} \\ \mathbf{h}_{22} & -\mathbf{g}_{22} & \mathbf{h}_{24} & -\mathbf{g}_{24} \\ \mathbf{h}_{32} & -\mathbf{g}_{32} & \mathbf{h}_{34} & -\mathbf{g}_{34} \\ \mathbf{h}_{42} & -\mathbf{g}_{42} & \mathbf{h}_{44} & -\mathbf{g}_{44} \end{bmatrix} \begin{Bmatrix} \mathbf{u}_2 \\ \mathbf{p}_2 \\ \mathbf{u}_4 \\ \mathbf{p}_4 \end{Bmatrix}$$

$$= \begin{bmatrix} -\mathbf{h}_{11} & \mathbf{g}_{11} & -\mathbf{h}_{13} & \mathbf{g}_{13} \\ -\mathbf{h}_{21} & \mathbf{g}_{21} & -\mathbf{h}_{23} & \mathbf{g}_{23} \\ -\mathbf{h}_{31} & \mathbf{g}_{31} & -\mathbf{h}_{33} & \mathbf{g}_{33} \\ -\mathbf{h}_{41} & \mathbf{g}_{41} & -\mathbf{h}_{43} & \mathbf{g}_{43} \end{bmatrix} \begin{Bmatrix} \mathbf{U}_1 \\ \mathbf{P}_1 \\ \mathbf{P}_3 \\ \mathbf{P}_3 \end{Bmatrix} = \begin{Bmatrix} \mathbf{f}_1 \\ \mathbf{f}_2 \\ \mathbf{f}_3 \\ \mathbf{f}_4 \end{Bmatrix}. \tag{13}$$

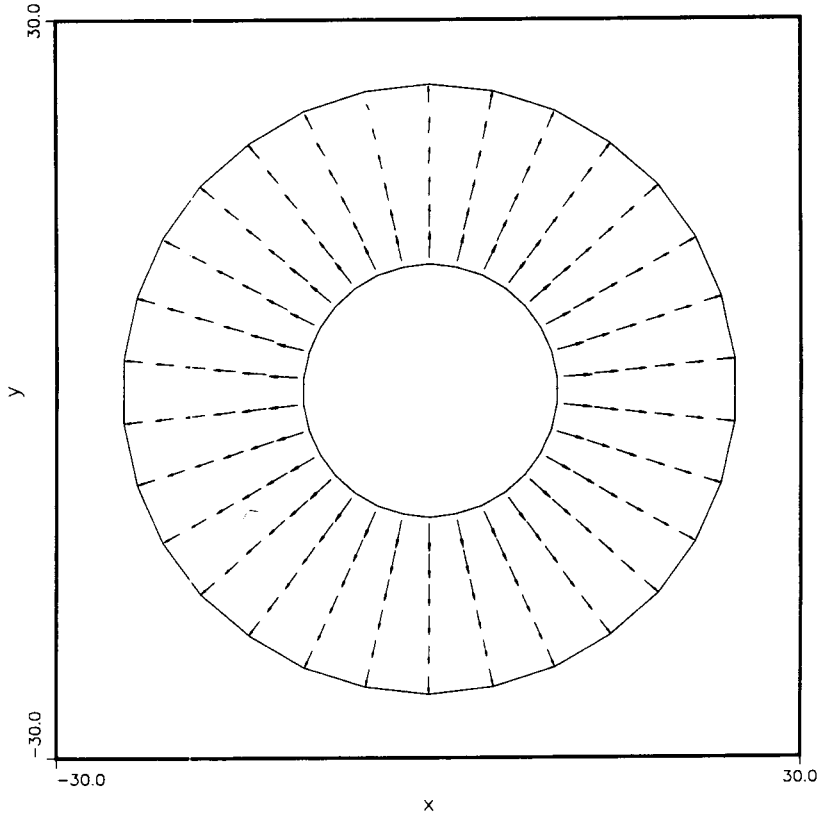

Fig. 3b. Vector displacement field from the ill-posed analysis of an annular pressurized disk: inner boundary over-specified.

The right-hand side vector $\{\mathbf{F}\}$ is known and the left-hand side remains in the form $[\mathbf{A}]\{\mathbf{X}\}$. Once the matrix $[\mathbf{A}]$ is solved, the entire **u** and **p** fields within the solid can be easily deduced from the integral formulation. The equation set $[\mathbf{A}]\{\mathbf{X}\} = \{\mathbf{F}\}$ resulting from our inverse boundary value formulation is highly singular and most standard matrix solvers will produce an incorrect solution. Nevertheless, singular value decomposition (SVD) methods [15] can be used to solve such problems accurately, although the number of unknowns in the equation set need not be the same as the number of equations [16] so that virtually any combination of boundary conditions will yield at least some solution. Additional equations may be added to the equation set if **u** measurements are known at locations within the solid in order to enhance the accuracy of the inverse steady boundary condition algorithm. A proper physical solution will be obtained if the number of equations equals or exceeds the number of unknowns. If the number of equations is less than the number of unknowns, the SVD method will find one solution, although it does not necessarily have to be the proper solution from the physical point of view [16].

ACCURACY OF THE BEM ELASTOSTATICS ANALYSIS CODE

We have used quadratic isoparametric interpolation functions for x and y coordinates and for **u** and **p** on each of the boundary panels in our two-dimensional elastostatics (plane strain) analysis code. The accuracy of this code was tested on a rectangular tensile specimen that was 5.0 cm long by 1.0 cm wide. The long sides of the specimen was discretized with five quadratic surface panels each 1.0 cm in length and the top and bottom sides had two panels each 0.50 cm in length. The top and bottom of the specimen were loaded with a uniform tensile stress of $P_y = 100\ \mathrm{N\,cm^{-2}}$. The two vertical sides were specified to have surface tractions of zero. The midpoints of the side walls were fixed with a zero vertical displacement ($U_y = 0$). The shear modulus was specified to be $G = 5.472 \times 10^8\ \mathrm{N\,cm^{-2}}$ and Poisson's ratio was $\nu = 0.345$. The two-dimensional elastostatics BEM code was solved for the displacement and stress fields within the specimen. The computed y-component of the displacement was uniform as expected and had a linear variation from zero to 0.00117 cm at the ends. The analytic solution from strength of materials gives a maximum displacement

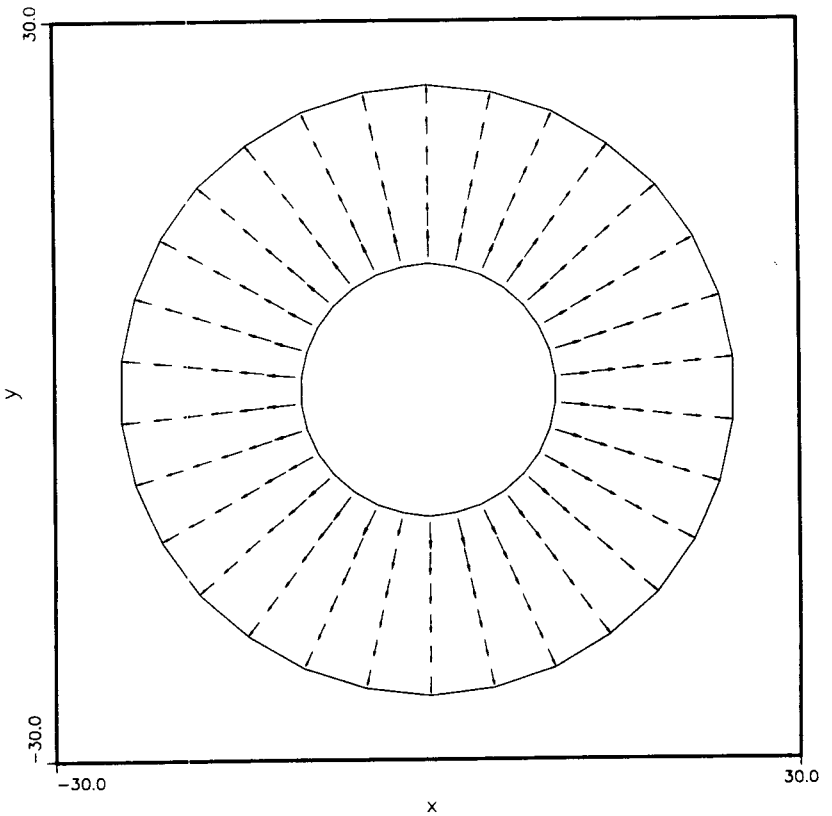

Fig. 3c. Vector displacement field from the ill-posed analysis of an annular pressurized disk: outer boundary over-specified.

of 0.00125 cm, although this is only a linearized analytic solution and it is not exact. The x-component of displacement varied linearly from 0 at the centerline to a maximum deformation of -8.0×10^{-4} cm at the vertical side walls.

ACCURACY OF THE BEM INVERSE BOUNDARY CONDITION CODE

The accuracy of the inverse boundary condition code was verified for the same tensile specimen as that of the previous test case. The boundary conditions were ill-posed such that both the displacement and traction vectors were known on the top, bottom and left sides of the rectangular plate. Elsewhere on the surface and on the right vertical side, no boundary conditions were specified. The inverse elastostatics BEM code predicted displacement and stress fields that were in error by about 1.0% on average compared to the numerical results of the previous analysis.

PRESSURIZED CIRCULAR CAVITY WITHIN AN INFINITE DOMAIN

The capability of the BEM in handling infinitely large domains was demonstrated for the case of a pressurized circular cavity. The wall of the cavity was discretized with 12 quadratic panels. The internal pressure was specified to be $P_r = 100\ \mathrm{N\,mm^{-2}}$ and the radius of the cavity was $r = 2.9745$ mm. The shear modulus was $G = 9.5 \times 10^4\ \mathrm{N\,mm^{-2}}$ and Poisson's ratio was $\nu = 0.1$, The x-displacements were fixed to zero at two nodes located at 90 and 270° measured from the x-axis. In addition, a single y-displacement was fixed to zero at the boundary node located at 0°. The stress analysis using the quadratic BEM predicted a radial displacement vector field shown in Fig. 1 with a maximum deflection of 0.002 mm on the boundary. Figure 2a shows a contour plot of lines of constant stress σ_{xx}.

The results of this analysis were then used for the boundary conditions prescribed on the ill-posed problem. The second and fourth quadrant boundaries of the circular cavity were specified with both displacements and tractions, while nothing was specified on the first and third quadrant circular boundaries. The inverse BEM elastostatics code predicted a displacement field that was in error by only about 0.03% compared to the prevous well-posed numerical analysis (Fig. 1). Figure 2b illustrates the equal stress contours, σ_{xx}, obtained by the inverse boundary value approach. The error between the numerically computed stress field of the inverse ill-posed problem and the direct well-posed problem was on average 0.5%.

ANNULAR CIRCULAR DISK

The inverse BEM algorithm was then tested on an infinitely long thick-walled pipe subject to an internal gauge pressure. The shear modulus for this problem was $G = 8.0 \times 10^4\ \mathrm{N\,mm^{-2}}$ and Poisson's ratio was $\nu = 0.25$. The radius of the inner surface of the pipe was 10 mm and the outer radius was 25 mm. The inner and outer boundaries were discretized with 12 quadratic panels each. The internal gauge pressure was specified to be $P_r = 100\ \mathrm{N\,mm^{-2}}$, while the outer boundary was specified with a zero surface traction. The two-dimensional elastostatics analysis boundary

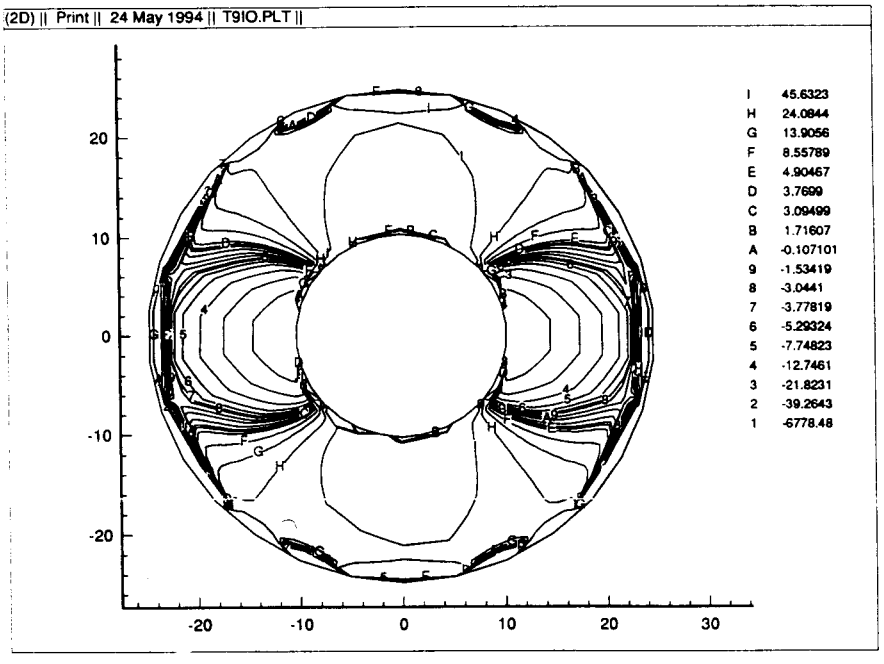

Fig. 4. Contours of constant stresses, σ_{xx}, from the well-posed analysis of an annular pressurized disk.

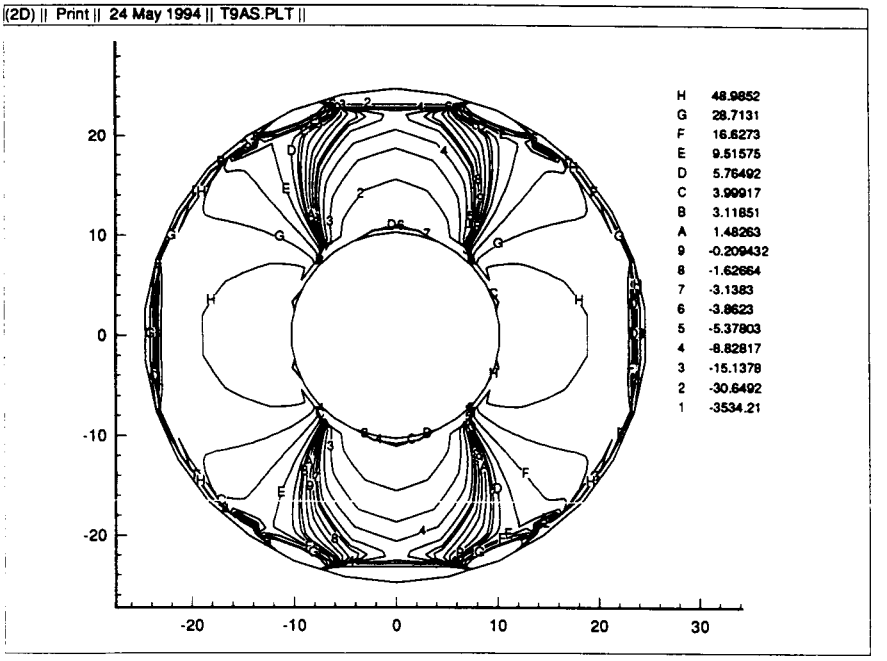

Fig. 5a. Contours of constant stresses, σ_{yy}, from the well-posed analysis of an annular pressurized disk.

element algorithm computed the displacement and stress fields within the circular annular domain. Figure 3a illustrates the radial displacement vector field with lengths of the arrows corresponding to the scaled magnitudes of the local deformations. Figures 4, 5a and 6a are contour plots of constant values of σ_{xx}, σ_{yy} and σ_{xy}, respectively that were computed using the analysis version of our second-order accurate BEM elastostatic code. The numerical results of this well-posed boundary value problem were then used as boundary conditions applied to the following two ill-posed problems.

First, the displacement vectors computed on the inner circular boundary were applied as over-specified boundary conditions in addition to the surface tractions already enforced there. At the same

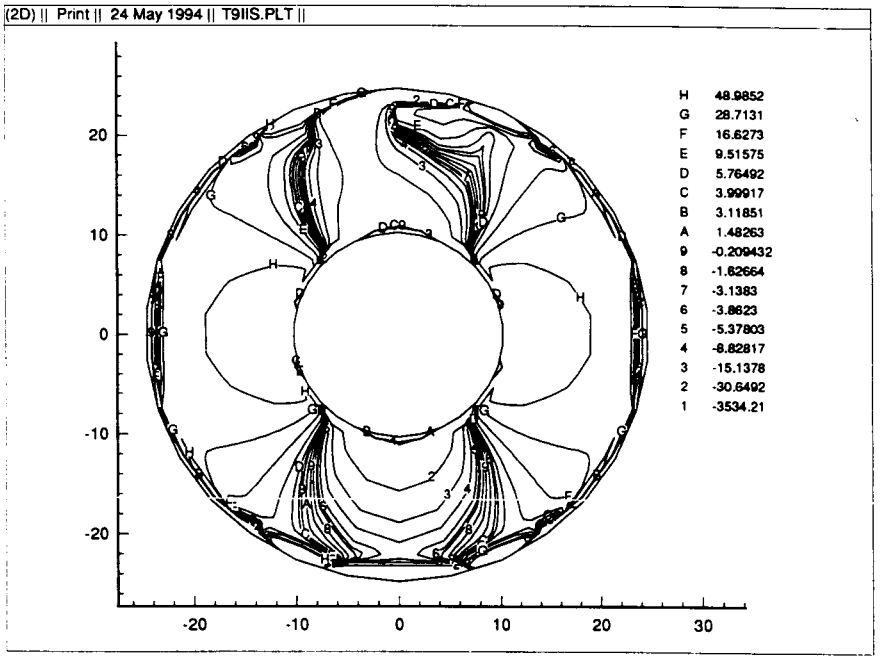

Fig. 5b. Contours of constant stresses, σ_{yy}, from the ill-posed analysis of an annular pressurized disk: inner boundary over-specified.

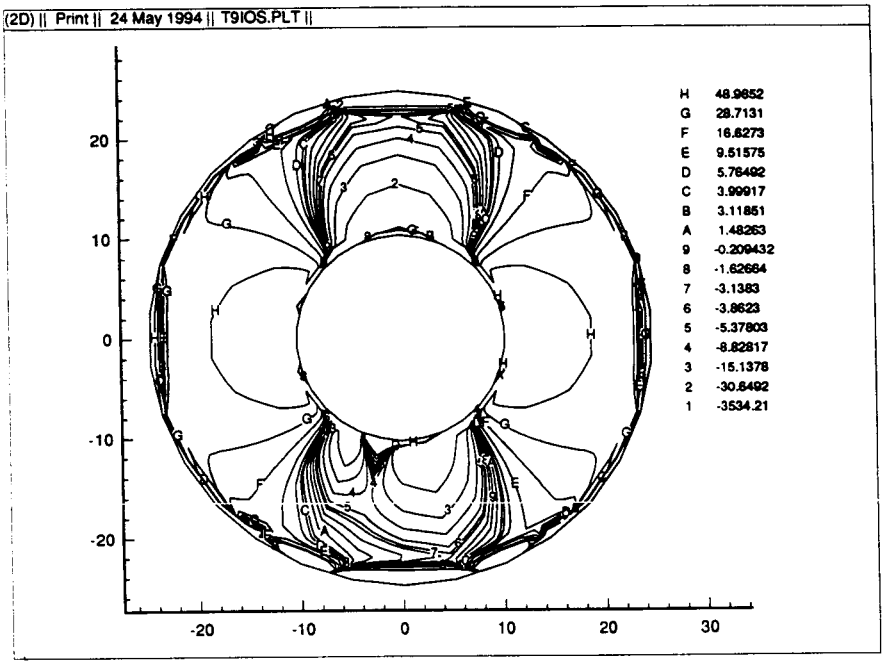

Fig. 5c. Contours of constant stresses, σ_{yy}, from the ill-posed analysis of an annular pressurized disk: outer boundary over-specified.

time nothing was specified on the outer circular boundary. Figure 3b shows the numerically computed radial displacement vector field for this inverse boundary value problem which was less than 1.0% in error compared to the well-posed analysis. Figures 5b and 6b are the contour plots of σ_{xx} and σ_{xy}, respectively, that were obtained with our inverse boundary value code. These stresses averaged a much larger error, about 3.0%, with some asymmetry in the stress field, when compared with the analysis results (Figs 5a and 6a). Next, the displacement vectors computed on the outer circular boundary by the well-posed numerical analysis were used to over-specify the outer circular boundary. At the same time nothing was specified on the inner circular boundary. Figure 3c shows the displacement field and

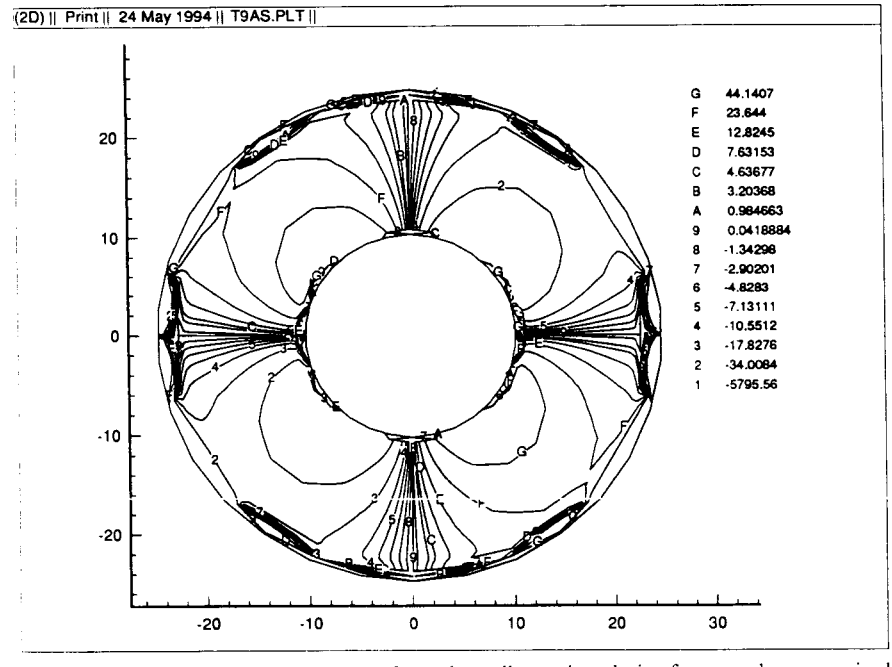

Fig. 6a. Contours of constant stresses, σ_{xx}, from the well-posed analysis of an annular pressurized disk.

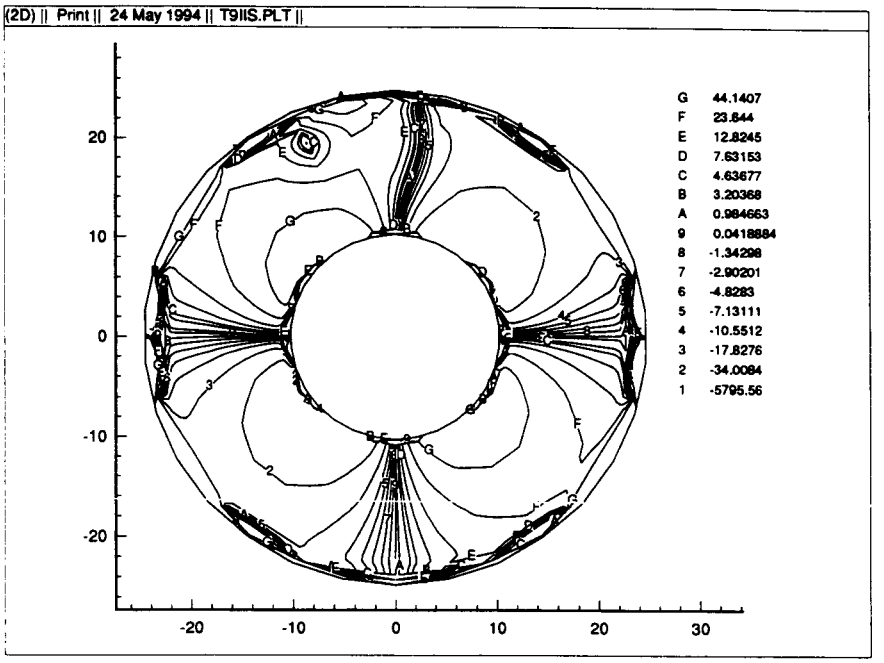

Fig. 6b. Contours of constant stresses, σ_{xx}, from the ill-posed analysis of an annular pressurized disk: inner boundary over-specified.

Figs 5c and 6c are the contour plots of σ_{yy} and σ_{xy}, respectively, as computed by the inverse BEM technique. The inner surface deformations were in error by less than 0.1%, while the stresses averaged less than a 1.0% error as compared to the analysis results.

Note that there is a large discrepancy in the error magnitudes between these two inverse problems. It seems that an over-specified outer boundary produces a more accurate solution than one having an over-specified inner boundary. It was also shown [1–5] that as the over-specified boundary area or the resolution in the applied boundary conditions were decreased, the amount of over-specified data also decreases, and thus the accuracy of the inverse boundary value technique deteriorates.

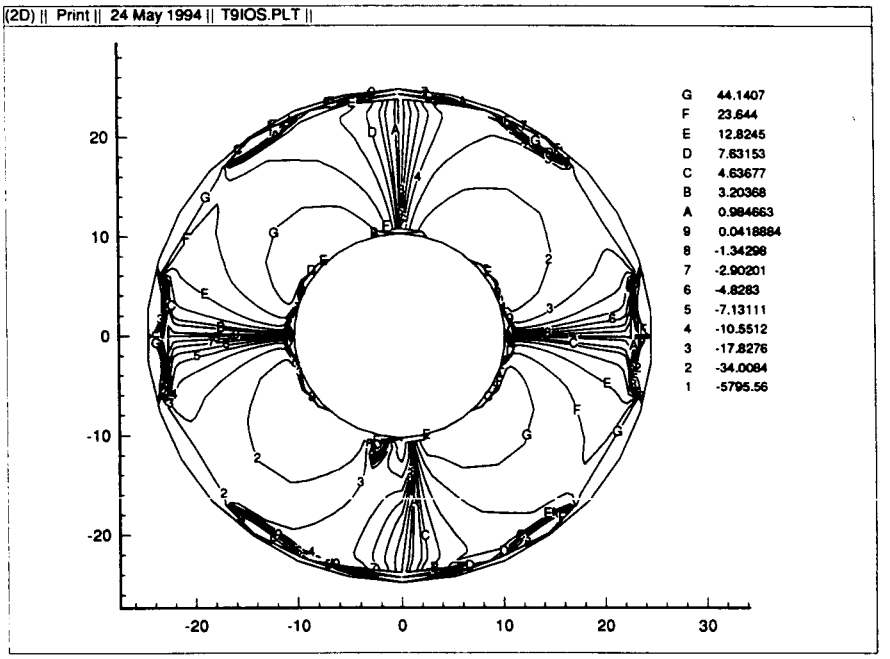

Fig. 6c. Contours of constant stresses, σ_{xy}, from the ill-posed analysis of an annular pressurized disk: outer boundary over-specified.

CONCLUSIONS

A new method has been developed that is capable of directly determining unknown steady boundary conditions (boundary surface tractions and deformations) on surfaces of solids where such quantities are unknown. This means that given any over-specified boundary conditions (such as tractions and deformations on surfaces where such data are readily available), the algorithm computes the stress and deformation fields within the solid and any unknown tractions and deformations on surfaces where these values are unavailable. A two-dimensional steady-state BEM program has been developed to perform automatic non-iterative determination of both tractions and deformations on parts of the interior and exterior boundaries of the solid. Numerical results were in excellent agreement with the analytic values in the regions relatively close to the over-specified data, but deteriorated as the amount of over-specified data was decreased. Our method is very fast since it is not iterative. For a typical two-dimensional BEM analysis or inverse boundary value run it consumes only seconds on an advanced personal computer.

Acknowledgements—Authors would like to thank Mr Norman F. Foster for his help with computer graphics and to Apple Computer for the donated equipment.

REFERENCES

1. T. J. Martin and G. S. Dulikravich, A direct approach to finding unknown boundary conditions in steady heat conduction. *Proc. 5th Annual Thermal and Fluids Workshop*, NASA CP-10122, pp. 137–149, NASA Lewis Research Center, Cleveland, OH (1993).
2. T. J. Martin and G. S. Dulikravich, Inverse determination of temperatures and heat fluxes on inaccessible surfaces. In *Boundary Element Technology IX* (Edited by C. A. Brebbia and A. Kassab), pp. 69–76. Computational Mechanics Publications, Southampton.
3. T. J. Martin and G. S. Dulikravich, Finding unknown surface temperatures and heat fluxes in steady heat conduction. *4th InterSociety Conf. Thermal Phenomena in Electronic Systems (I-THERM IV)* (Edited by A. Ortega and D. Agonafer), pp. 214–221, Washington, DC (1994).
4. G. S. Dulikravich and T. J. Martin, Inverse problems and shape design in heat conduction. *Proc. 2nd Int. Symp. Inverse Problems in Engineering* (Edited by H. D. Bui and M. Tanaka), pp. 13–20. Balkema, Rotterdam (1994).
5. R. D. Throne and L. G. Olson, A generalized eigensystem approach to the inverse problem of electrocardiography, *IEEE Trans. biomed. Engng* **41**(6), 1–9 (1994).
6. L. M. Bezzera and S. Saigal, A boundary element formulation for the inverse elastostatics problem (IESP) of flaw detection. *Int. J. numer. Meth. Engng* **36,** 2189–2202 (1993).
7. A. J. Kassab, F. A. Moslehy and A. Daryapurkar, Detection of cavities by inverse elastostatics boundary element method: experimental results. In *Boundary Element Technology* (Edited by C. A. Brebbia and A. Kassab), pp. 85–92. Southampton (1994).
8. G. A. Dulikravich and T. J. Martin, Inverse design of super-elliptic cooling passages in coated turbine blade airfoils, *AIAA J. Thermophys. Heat Transfer* **8**(2), 288–294 (1994).
9. J. V. Beck, B. Blackwell and C. R. St Clair Jr, *Inverse Heat Conduction: Ill-Posed Problems*. Wiley, New York (1985).
10. B. Dorri, Inverse heat conduction analysis using boundary integral and finite element formulations. *AIAA–ASME Thermophysics and Heat Transfer Conf., June* 18–20, 1990, *Seattle, WA, Symp. Numerical Heat Transfer* (Edited by K. Vafai and J. L. S. Chen), ASME, HTD-Vol. 130, pp. 87–93 (1990).
11. T. R. Hsu, N. S. Sun, G. G. Chen and Z. L. Gong, Finite element formulation for two-dimensional inverse heat conduction analysis. *ASME J. Heat Transfer* **114,** 553–557 (1992).
12. D. A. Murio, *The Mollification Method and the Numerical Solution of Ill-Posed Problems*. Wiley, New York (1993).
13. C. A. Brebbia and J. Dominguez, *Boundary Elements, An Introductory Course*. McGraw-Hill, New York (1989).
14. C. A. Brebbia, *The Boundary Element Method for Engineers*. Wiley, New York (1978).
15. W. H. Press, S. A. Teukolsky, W. T. Vetterling and B. P. Flannery, *Numerical Recipes in FORTRAN*, 2nd Edn. Cambridge University Press (1992).
16. M. Okuma and S. Kukil, Correction of finite element models using experimental modal data for vibration analysis. In *Inverse Problems in Mechanics* (Edited by K. Kubo), pp. 204–211. Atlanta Technology, Atlanta, GA (1993).